Technical note

Optimization of DOAS settings for BrO fitting from SCIAMACHY nadir spectra - Comparison with GOME BrO retrievals

I. De Smedt, M. Van Roozendael, T. Jacobs

Belgian Institute for Space Aeronomy (IASB-BIRA), Brussels, Belgium

Table of Content

1. Introduction and purpose

SCIAMACHY (SCanning Imaging Absorption spectroMeter for Atmospheric CartograpHY) is a passive remote sensing spectrometer observing backscattered, reflected, transmitted or emitted radiation from the atmosphere and Earth's surface, in the wavelength range between 240 and 2380 nm. The instrument flies on board of the ESA ENVISAT platform which was launched on 1 March 2002. SCIAMACHY primary mission objective is to perform global measurements of trace gases in the troposphere and in the stratosphere. The solar radiation transmitted, backscattered and reflected from the atmosphere is recorded at moderately high resolution (0.2 μm to 0.5 μm) over the range 240 nm to 1700 nm, as well as in selected regions between 2.0 μm and 2.4 μm. Owing to its resolution and the wide wavelength range covered, SCIAMACHY has the ability to detect many atmospheric trace gases (O_3, BrO, OClO, ClO, SO_2, H_2CO, NO_2, CO, CO_2, CH_4, H_2O, N_2O). The large wavelength is also ideally suited for the determination of aerosols and clouds.

The technique used to retrieve trace gases from SCIAMACHY spectra in the UV/Visible spectral range is the Differential Optical Absorption Spectroscopy (DOAS, Platt, 1994). This technique has been widely used for the retrieval of atmospheric gases from the ground, from balloons and from space. In the present document, we focus on the optimization of analysis settings for BrO slant column retrieval from SCIAMACHY nadir observations. This work has been performed as part of the ESA-ESRIN TEMIS project and in support of the SCIAMACHY verification team. Starting from the 5-years experience acquired with BrO evaluations from GOME spectra, the problems specific to SCIAMACHY are described and possible solutions are proposed and tested. Details are provided as regards testing procedures applied using the last version of the SCIAMACHY Level 0 to 1 Processor as well as different versions of the key data.

2. BrO Slant Columns Retrieval from GOME

As a baseline, the inversion of BrO slant columns from GOME is performed in the 344.7-359 nm spectral range. Other settings basically follow the recommendations issued in the extensive study of Aliwell et al. [2002]. The BrO absorption cross-sections used are those from Wilmouth et al. [1999], convolved to the GOME resolution, which is derived as part of the retrieval algorithm. The DOAS procedure accounts for the GOME undersampling [Chance, 1998]. More details on the DOAS procedure applied can be found in Van Roozendael et al. [1999].

Fitting interval:	344.7-359 nm
Molecular absorption cross-sections:	BrO [Wilmouth et al., 1999]
	O_3 221K [Burrows et al., 1999]
	O_3 241K [Burrows et al., 1999]
	NO_2 [Burrows et al., 1998]
	O_4 [Greenblatt et al., 1990]
	OClO [H. Kromminga et al., 1999]
	H_2CO [Cantrell et al., 1989]
Additional terms/corrections:	Polynomial (order 3)
	Ring cross-sections [Vountas, 1998]
	Undersampling [Chance, 1998]
	Offset (constant + slope)
	Shift of O_3 and NO_2 cross-sections (0.03nm)
	Wavelength calibration based on Kurucz solar spectrum.

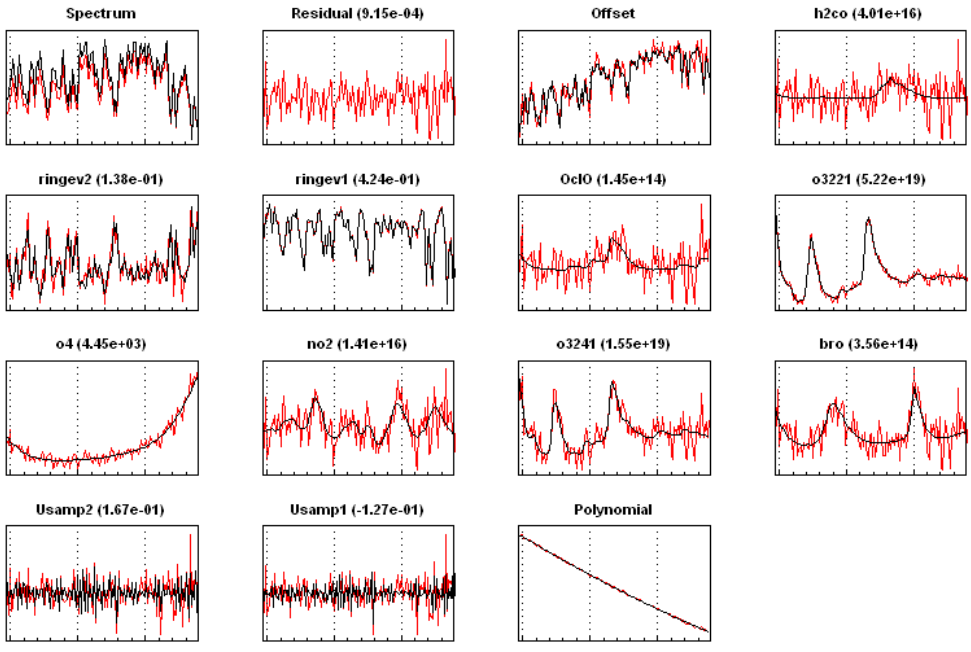

Figure 1: Example of 1 pixel fit process. Black lines are laboratory references and red lines are the fit results.

3. Slant Columns Retrieval from SCIAMACHY

The aim is to derive consistent GOME and SCIAMACHY BrO slant column products.

3.1 Choice of a fitting interval

Test retrievals, initially performed in the GOME fitting window (344.7-359nm), have revealed major problems due to the presence of a strong Wood's anomaly which occurs right in the middle of the SCIAMACHY channel 2. This anomaly leads to strong polarization-related spectral features (see Figure 2), which interferes with the BrO absorption structures. Concurrently, the signal to noise ratio is reduced due to the anomalously low grating efficiency around 350 nm (see Figure 3).

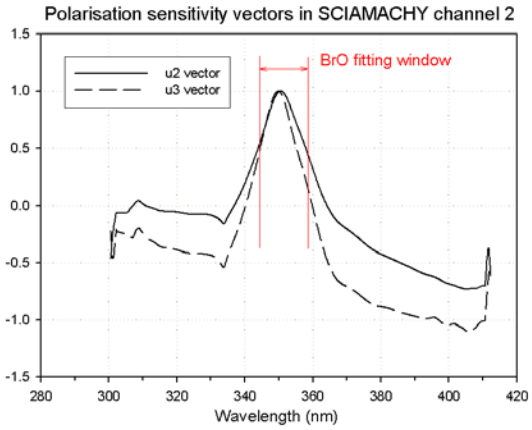

Figure 2: Polarisation feature

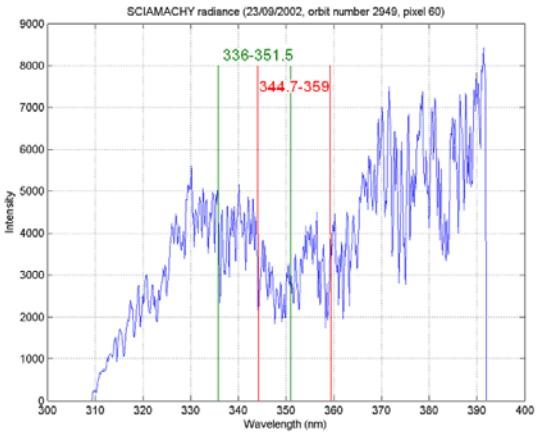

Figure 3: Poor S/N ratio in the BrO window

Attempts were made to reduce polarization-related artifacts by adding two polarization vectors u2 and u3, extracted from the SCIAMACHY key data set, in the DOAS fit procedure. With this empirical correction, large offset errors could generally be reduced but the noise remains unacceptably high in all cases (Figure 4).

SCIA data fitted in GOME window | **Same, + u2 and u3 vectors**

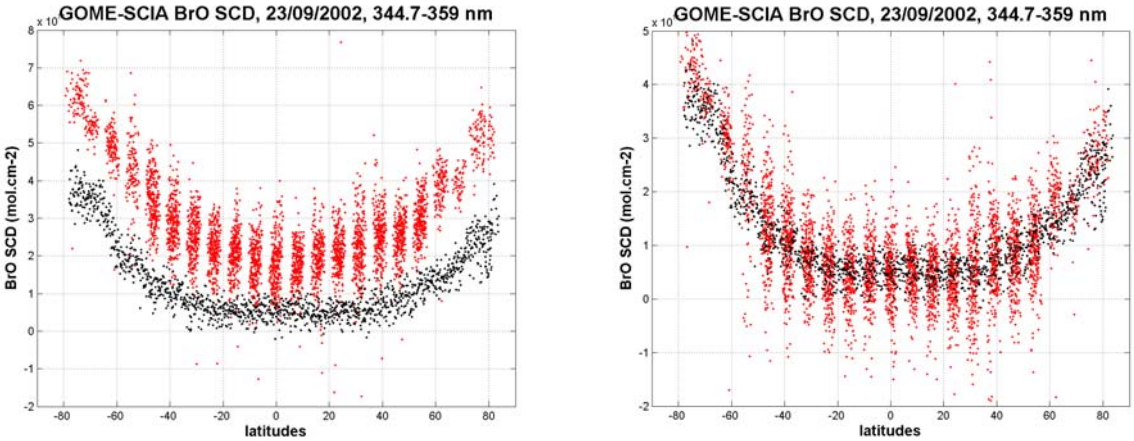

Figure 4: Fit of BrO without and with polarisation vectors fit.

Therefore an alternative fitting window (UV-shifted, initially 336-347 nm) has been searched and tested (see the cross-sections in the two windows showed on Figure 5). In this region, the polarization features are smoother and therefore have a smaller impact on the accuracy of the DOAS procedure.

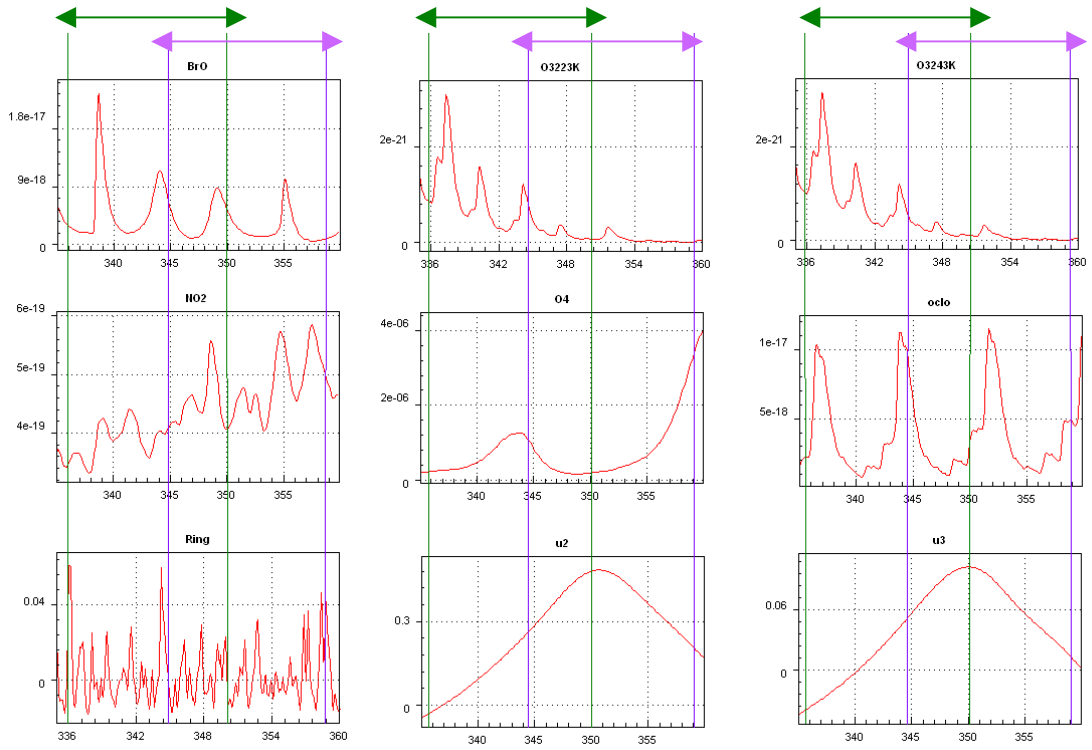

Figure 5: SCIA cross-sections between 335-360 nm

The GOME-SCIAMACHY consistency was found to be good in this UV-shifted window (see Figure 6). However to use it with confidence for SCIA, we also had to check whether GOME spectra analyses give consistent results in both windows. Indeed, radiative transfer calculations show that the BrO air mass factors should not vary by more than 1% between 340 and 350 nm.

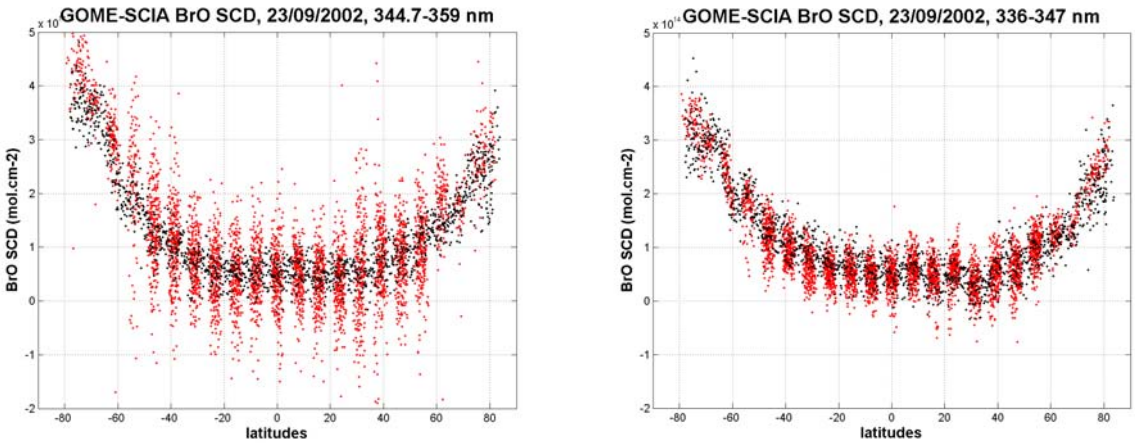

Figure 6: SCIA data fitted in shifted window (336-347 nm)

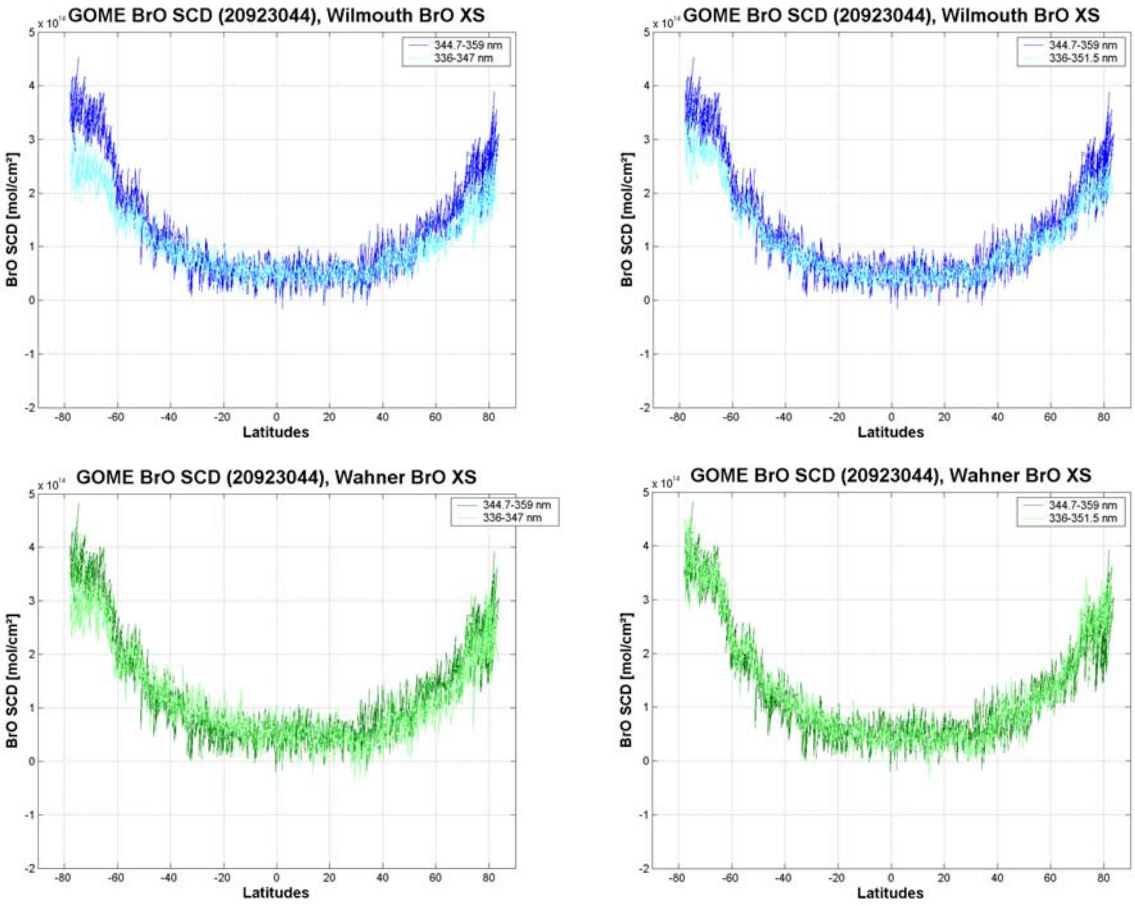

Figure 7: Comparison between different fitting windows (344.7-359, 336-347, 336-351.5 nm), for two BrO XS (Wilmouth and Wahner).

Two BrO cross-sections have been tested (see details in section 3.2). For both of them, the best compromise between optimal consistency for GOME in the two windows, and best fit for SCIAMACHY was found in the adjusted window 336-351.5 nm (see Figure 8). This interval includes three bands of BrO as can be seen from Figure 5.

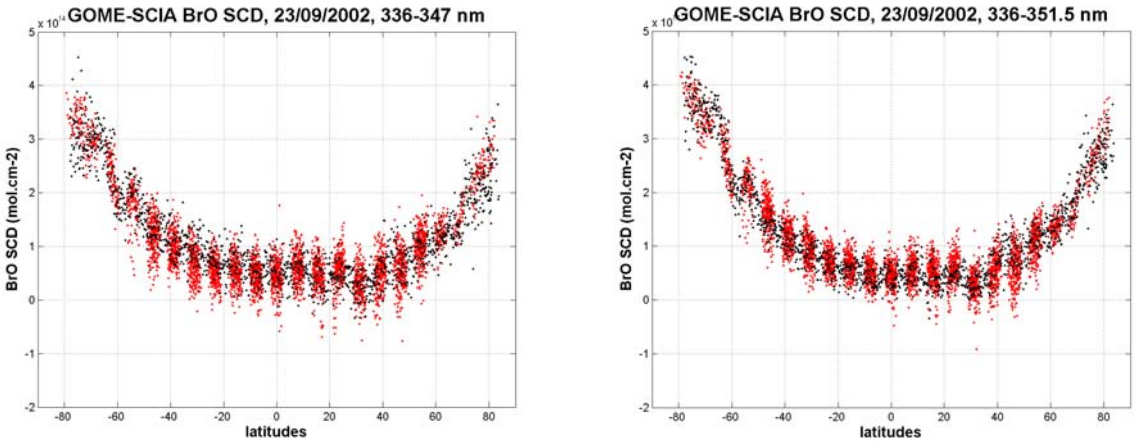

Figure 8: Comparison of SCIA results in the two windows 336-347 and 336-351.5 nm with corresponding GOME analysis.

For SCIAMACHY as well, results were found to be better in the 336-351.5 nm than in the initial UV-shifted interval (336-347 nm). The consistency is better at high latitudes and the noise is reduced. In contrast to the 336-347 window, polarization vectors u2 and u3 have to be fitted. The reduction in the number of degrees of freedom due to adding the two empirical vectors is largely compensated by the larger width of the fitting interval. Extensive tests also show that moving to the larger fitting window (336-351.5 nm) has no impact on the quality of the fit.

Regarding GOME results, the UV-shifted window tends to show greater instability over time than the classical one, however the results are globally consistent in the two windows.

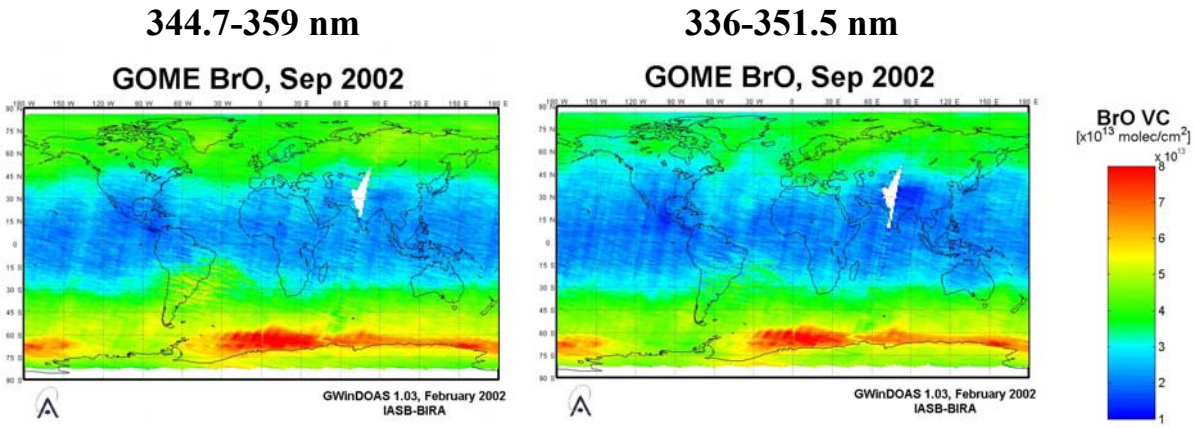

3.2 BrO Cross-section

Two BrO cross-sections have been tested: Wahner [Wahner et al., 1988] and Wilmouth [Wilmouth et al., 1999]. In the classical BrO fitting interval (344.7-359 nm) the two cross-sections give consistent results, as can be judged from Figure 9. The Wilmouth et al. cross-sections had been chosen for GOME analysis because of their resolution (0.15 nm) which matches better the resolution of the GOME instrument (0.17 nm in channel 2).

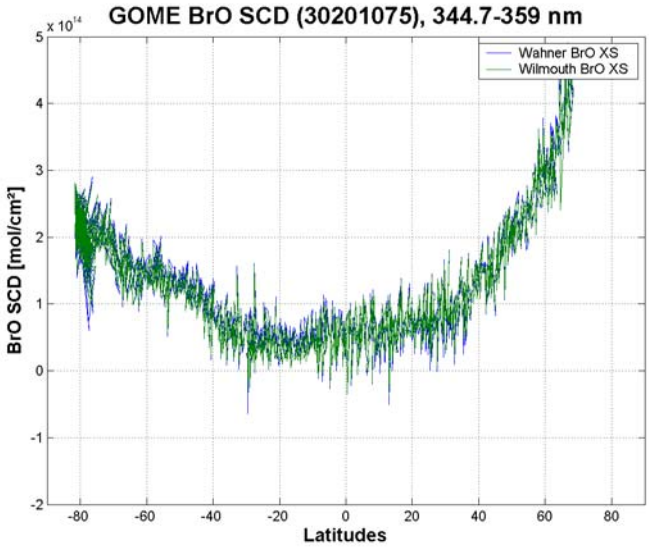

Figure 9: Comparison of the results obtained in the classical BrO interval, with Wahner and Wilmouth cross-sections.

In the UV-shifted window however, differences of the order of 20% are found when using one or the other BrO cross-section. It is the cross-section of Wahner that gives the best match between the two windows. However the use of the Wilmouth cross-section leads to reduced noise on the retrieved BrO slant columns.

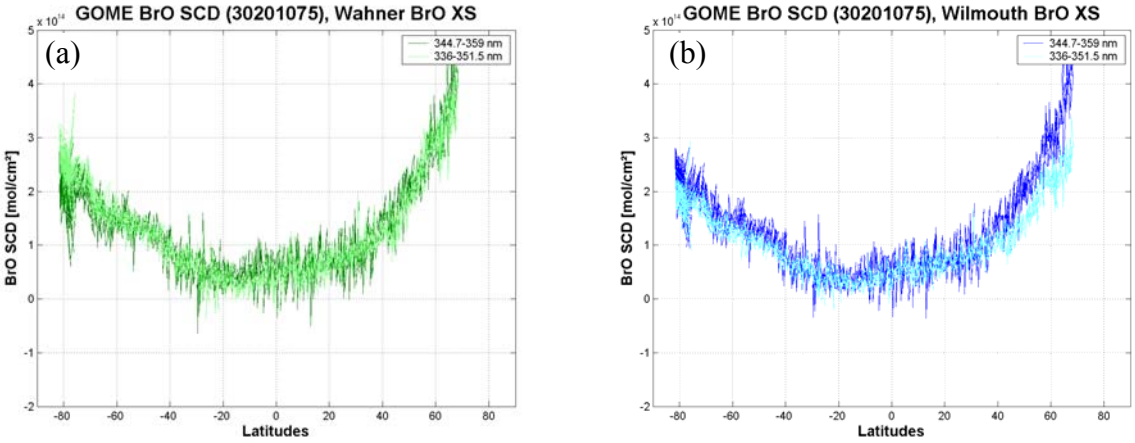

Figure 10: Comparison of GOME BrO SCD obtained in the classical BrO window (344.7-359 nm) and in the UV-shifted window (336-351.5 nm) with Wahner cross-sections (a) and Wilmouth cross sections (b).

From the above, it can be concluded that none of the presently available BrO cross-section laboratory data appears to be fully adequate for GOME and SCIAMACHY retrieval. To avoid inconsistencies with GOME, our current recommendation is to use the Wahner cross-sections for SCIA retrieval, keeping in mind however that this choice will not be optimal in terms of noise. Another possible option to empirically resolve the wavelength-dependent inconsistency of the Wilmouth BrO cross-sections is to apply a scaling factor to the Wilmouth data in the UV-shifted interval (Figure 11). An appropriate correction factor can be calculated by resolving the equation $X=A^{-1}*B$ separately in the two wavelength intervals, A and B being respectively the Wilmouth and Wahner BrO cross-sections. The ratio of the two scalars obtained with this equation in the two windows represents the correction that has to be applied to the Wilmouth cross-section in the UV-shifted window. This calculation leads to a correction factor of 0.83.

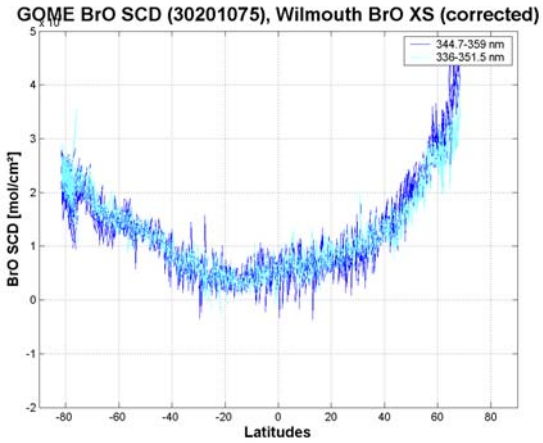

Figure 11: Comparison of GOME BrO SCD obtained in the classical BrO window (344.7-359 nm) and in the UV-shifted windows (336-351.5 nm) with the Wilmouth BrO cross section scaled by a factor 0.83.

Note that the inconsistency found using the Wilmouth cross-sections in the two fitting intervals is confirmed when comparing results of GOME and SCIAMACHY: SCIA retrievals using the Wahner cross-section gives better match with GOME (see Figure 12 and Figure 13). This further suggests that the problem comes from laboratory measurements of the cross-section rather than from an artefact of the GOME instrument.

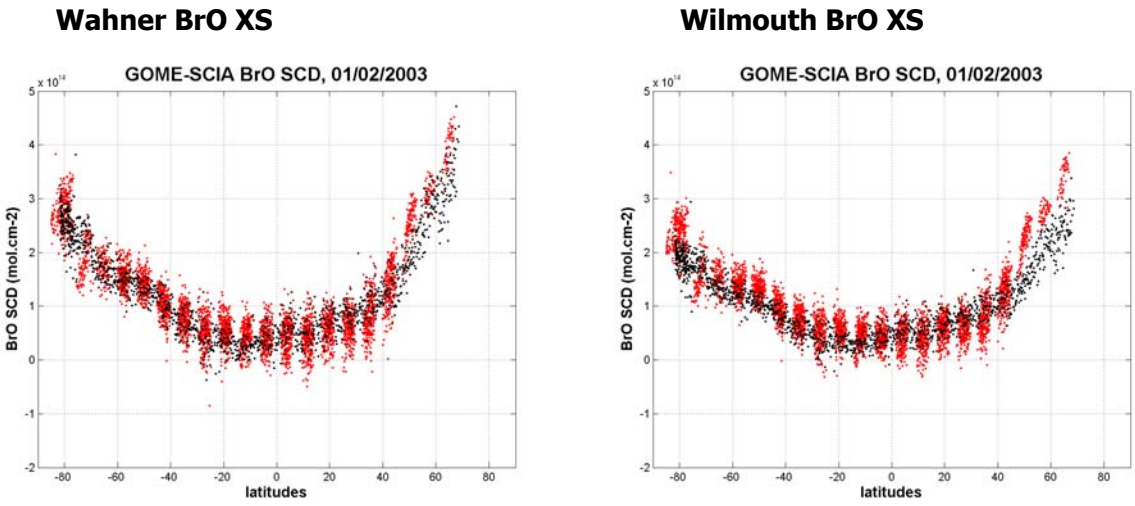

Figure 12 : Comparison between GOME and SCIA in the 336–351.5 nm window, for Wahner BrO cross-section and Wilmouth BrO cross-section.

3.3 GOME-SCIA comparison for February 2003

A comparison between BrO vertical columns derived, for the month of February 2003, from GOME and available spectra of SCIAMACHY (neither all days nor a total coverage for each day are available) is presented in Figure 13. In these plots, GOME values are baseline retrievals in the 344.7-359 nm interval, while SCIAMACHY data have been processed in the UV-shifted window (336-351.5 nm), first using the Wahner BrO cross-sections, second using the Wilmouth cross-sections. Best match with GOME is clearly obtained using the Wahner cross-section. Similarly, good matching with GOME can also be obtained using the Wilmouth cross-sections when these are scaled by 0.83 (see Figure 14).

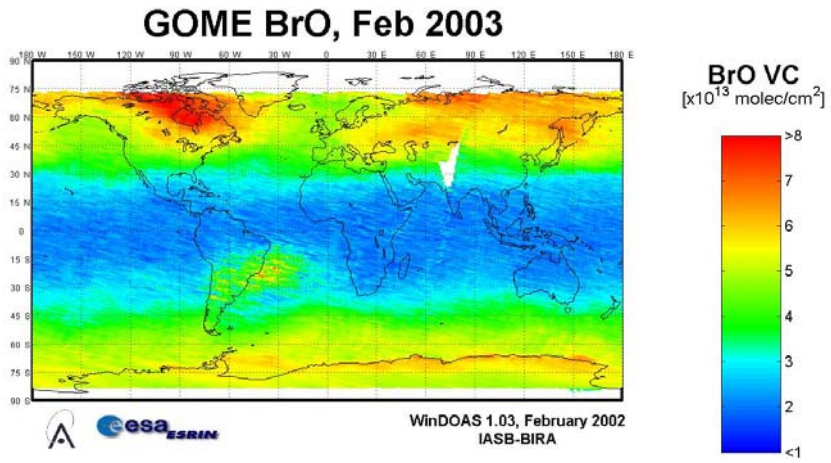

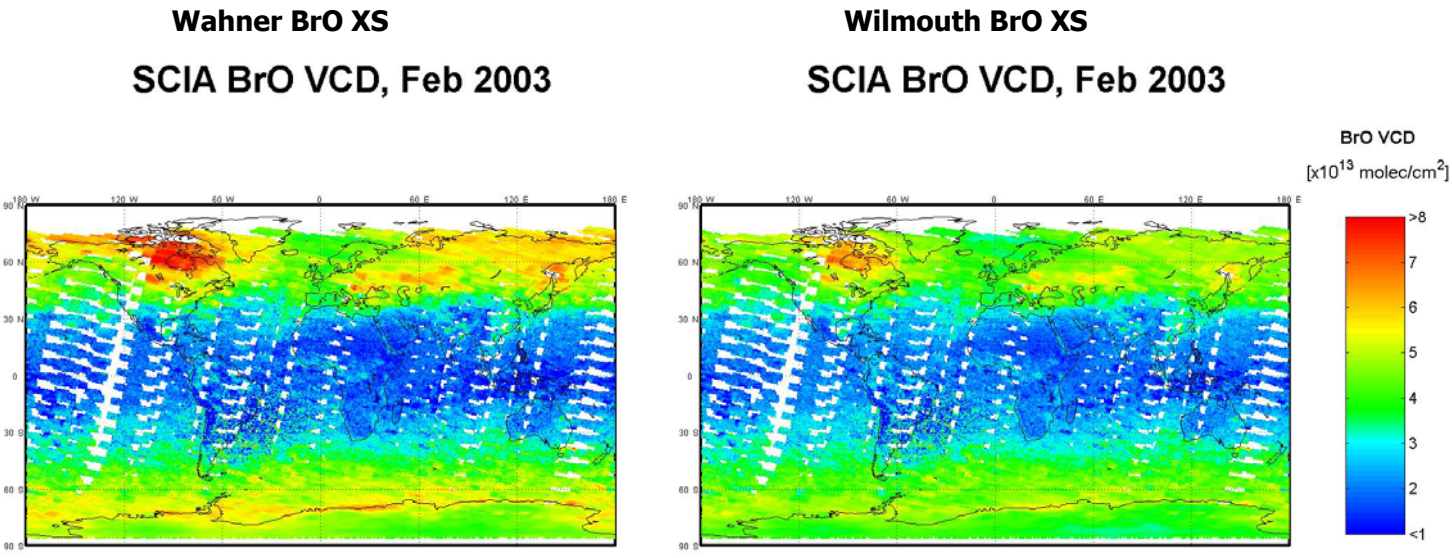

Figure 13: Monthly averaged BrO columns for February 2003 retrieved with GOME and available SCIA spectra, with respectively Wahner and Wilmouth BrO cross-sections

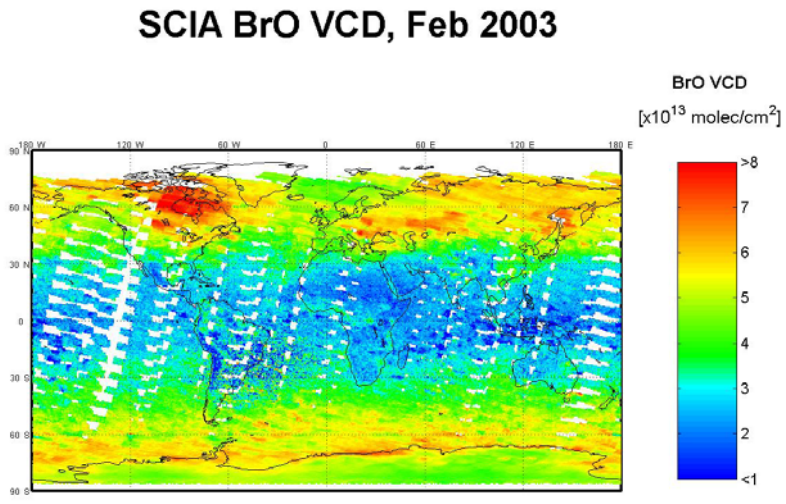

Figure 14: Monthly averaged BrO columns for February 2003 retrieved from available SCIAMACHY spectra using the Wilmouth BrO cross-section scaled by 0.83

3.4 Problem of the formaldehyde interference

In some cases (e.g. orbits crossing regions of strong biomass burning-related emissions), formaldehyde has to be included in the BrO fit in the 336-351.5 nm window, which increases the noise. This can be a problem for SCIAMACHY spectra because the noise can become unacceptable (Figure 15).

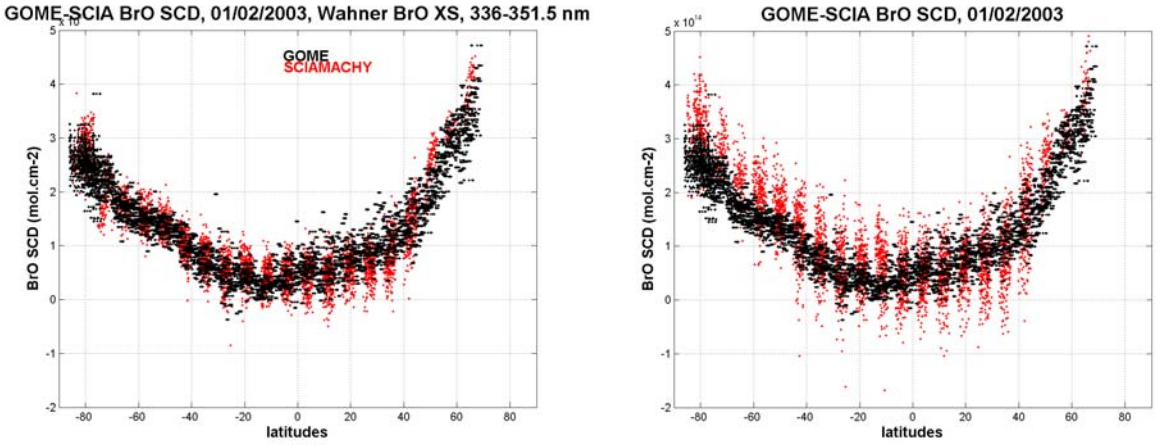

Figure 15: GOME-SCIA BrO SCD comparison without and with formaldehyde included in the fit.

Our current baseline for SCIAMACHY BrO analysis is to use the 336-351.5 nm fitting window, without inclusion of formaldehyde. According to results obtained so far, SCIAMCHY retrievals using these settings are generally in very good agreement with GOME. However more data are still needed to estimate the importance of not fitting for formaldehyde.

3.5 Recommended baseline settings for SCIAMACHY BrO slant column retrieval

Fitting interval:	336-351.5 nm
Molecular absorption cross-sections:	BrO [Wahner et al., 1988] O3 at 223K V2 [Bogumil et al., 1999] O3 at 243K V2 [Bogumil et al., 1999] NO2 at 243K V1 [Bogumil et al., 1999] OClO [Bogumil et al., 1999] O4 [Greenblatt et al., 1990]
Additional terms/corrections:	Polynomial (order 2) Ring cross-sections calculated using SCIATRAN model [Vountas, 1998] Polarization cross-sections [Key Data for SCIAMACHY processing] Offset (constant + slope) Wavelength calibration based on Kurucz solar spectrum.

Due to the current unavailability of reliable SCIAMACHY solar spectra, a radiance spectrum taken at the equator is currently used as reference spectrum. Further processing then follows according to GOME standard evaluations. A mean SCD value is calculated around the equator (0°±5°) for each day and then subtracted to attenuate the noise due to SCIA radiances. Afterwards an offset correction is applied, taking into account the BrO value generally admitted at the equator (5e13 mol/cm²).

3.6 Conclusion

The strong Wood's anomaly present in the channel 2 of SCIAMACHY prevents reliable BrO retrievals to be obtained in the fitting window (344.7-359 nm) used for GOME evaluations. SCIAMACHY nadir spectra are characterized in this wavelength region by strong polarization features and by a reduced signal to noise ratio around 340-360 nm. In order to bypass these difficulties, alternative BrO fitting windows have been explored. The 336-351.5 nm interval was found to offer best compromise, showing good consistency with GOME results in the usual 344.7-359 nm interval and, at the same time, optimal stability for SCIAMACHY. Similarly, for reasons of consistency with GOME retrievals, the Wahner BrO cross-section is preferred instead of Wilmouth data despite their lower resolution. Our recommendation for DOAS retrieval of BrO from SCIAMACHY is therefore to use a UV-shifted fitting interval (336-351.5 nm), with the Wahner BrO cross-sections (see detailed settings in section 3.5). Remaining small polarization features can be satisfactorily eliminated by adding two empirical polarization vectors fitted as part of the DOAS process.

This study has been performed in parallel with the Bremen BrO team (T.Wagner, O.Afe). The Bremen and IASB BrO evaluations from both GOME and SCIAMACHY data are fully consistent.

4. Verification data set: tests on the improvement of SCIAMACHY Level 0 to 1 processor and key data.

4.1 Definition of the different configurations presented

The aim of this section is to test the adjustment of L0/1B Processor and the new key data set. In the following tests, the number of the configuration will always refer to the following definitions:

Previous results:
Config. 1 : Processor 4.0, Nadir Key Data version 2.2
New processor, 3 versions of the key data
Config. 2 : Processor 4.02b, Nadir Key Data version 2.2
Config. 3 : Processor 4.02b, Nadir Key Data version 3.0
Config. 4 : Processor 4.02b, Nadir Key Data version 2.4

Test Orbits of 23/08/2002:

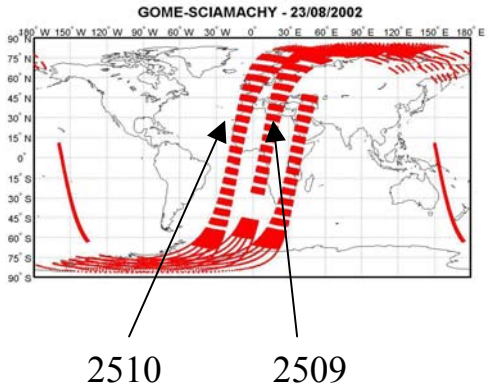

4.2 Radiances in SCIAMACHY channel 2: Woods anomaly:

The relative loss of intensity in the range 340-360 nm has been corrected in the new processor version (4.02b), however, the signal-to-noise problem will remain in the 340-350 nm window, regardless of the accuracy of the radiometric calibration.

No polarization correction during calibration:

Processor 4.0

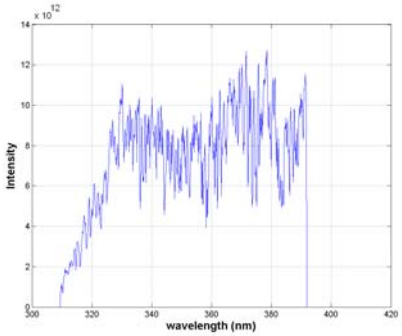

Processor 4.02b (version 3)

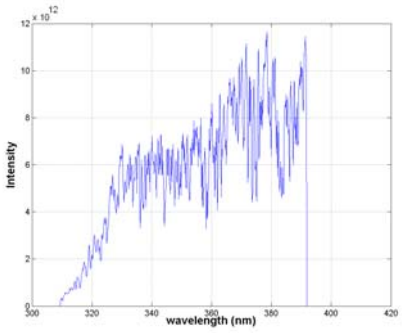

Polarization correction during calibration:

Processor 4.0

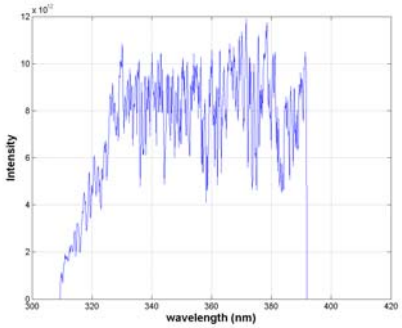

Processor 4.02b (version 3)

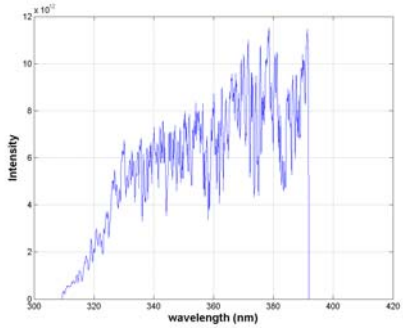

4.3 Orbit 2509 with polarization correction during calibration (options: 1,2,3,4,5,6,7)

4.3.1 Previous results (Config. 1, Processor 4.0, Nadir key data 2.2)

344.7-359 nm

with fit of u2 and u3

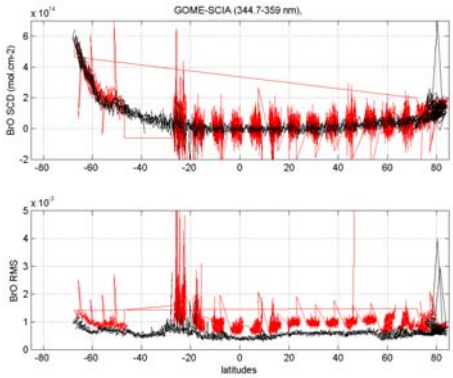

without fit of u2 and u3

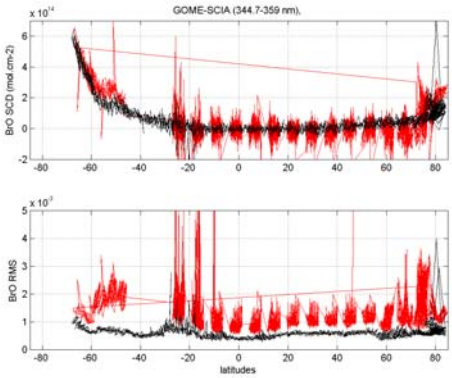

336-351.5 nm

with fit of u2 and u3

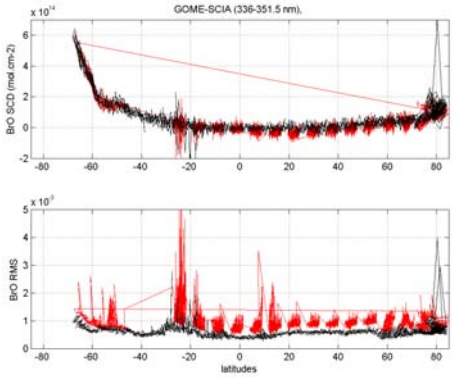

without fit of u2 and u3

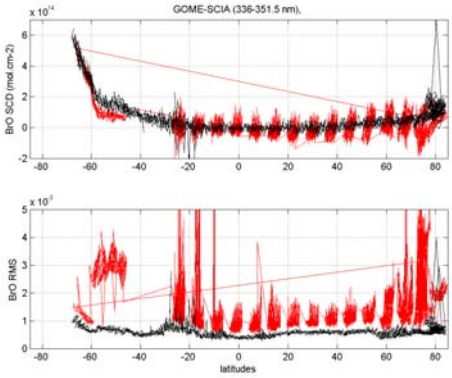

4.3.2 Key data version 1 (Config. 2, Processor 4.02b, Nadir key data 2.2)

344.7-359 nm

with fit of u2 and u3

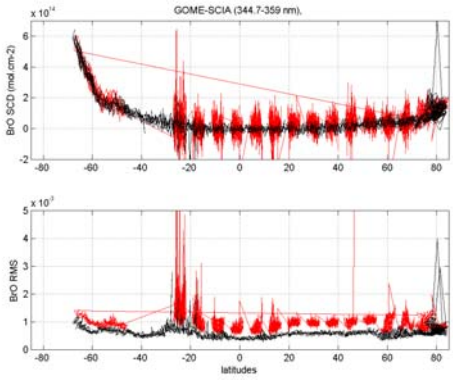

without fit of u2 and u3

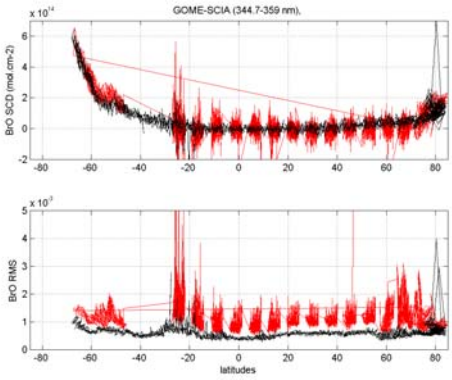

4.3.3 Key data version 2 (Config 3, Processor 4.02b, Nadir key data 3.0)

344.7-359 nm

with fit of u2 and u3

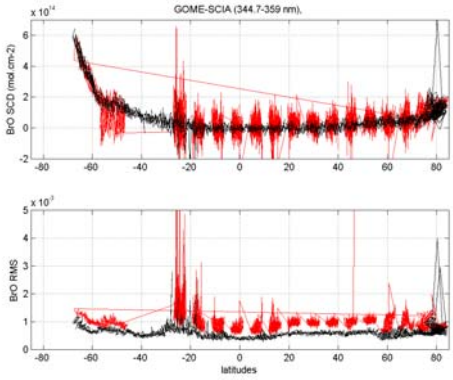

without fit of u2 and u3

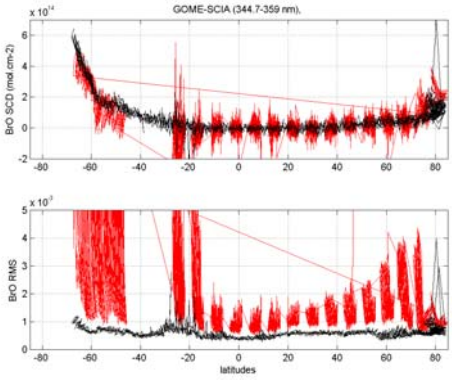

4.3.4 Key data version 3 (Config 4, Processor 4.02b, Nadir key data 2.4)

344.7-359 nm

with fit of u2 and u3

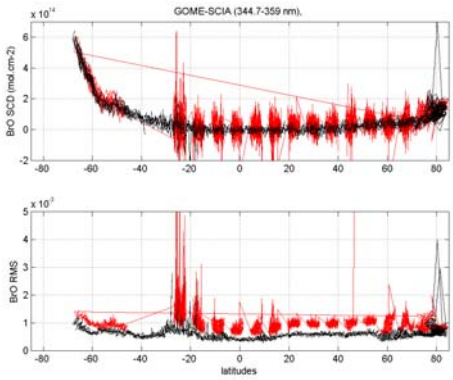

without fit of u2 and u3

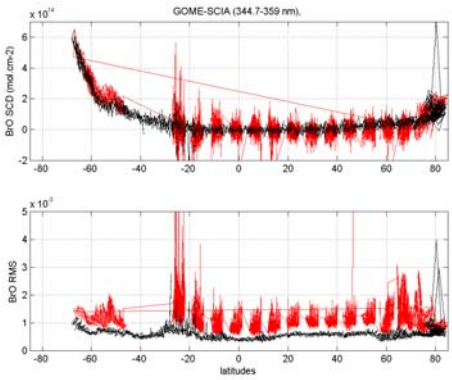

4.4 Orbit 2509 without polarization correction during calibration (options: 1,2,3,4,5,7)

4.4.1 Previous results (Config. 1, Processor 4.0b, Nadir key data 2.2)

344.7-359 nm

with fit of u2 and u3

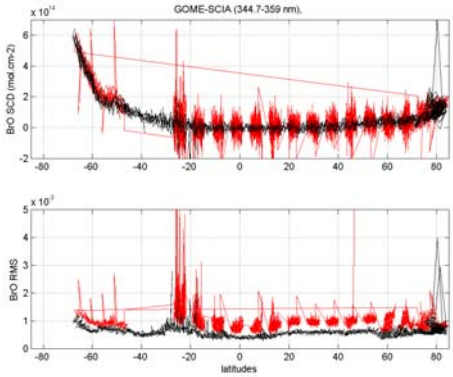

without fit of u2 and u3

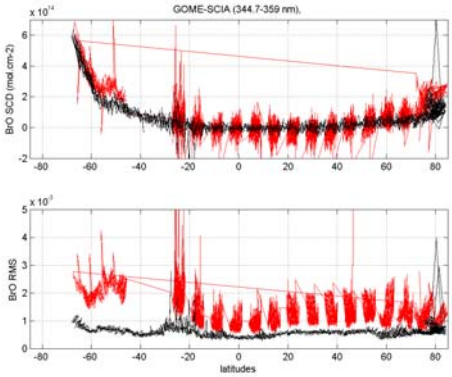

336-351.5 nm

with fit of u2 and u3

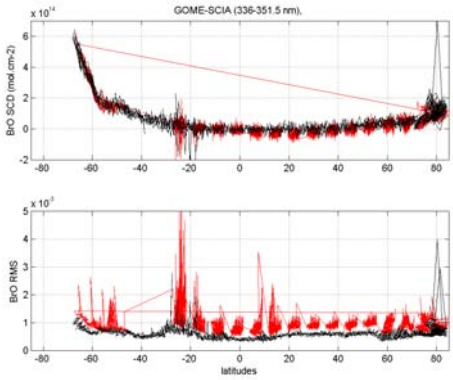

without fit of u2 and u3

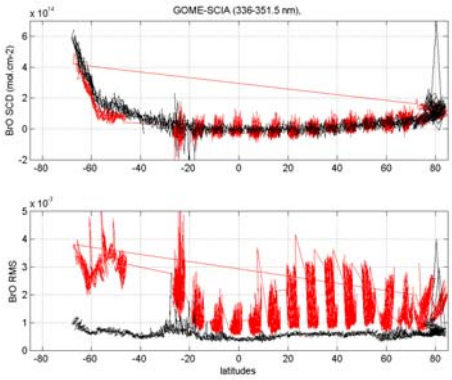

4.4.2 Key data version 1 (Config. 2, Processor 4.02b, Nadir key data 2.2)

344.7-359 nm

with fit of u2 and u3

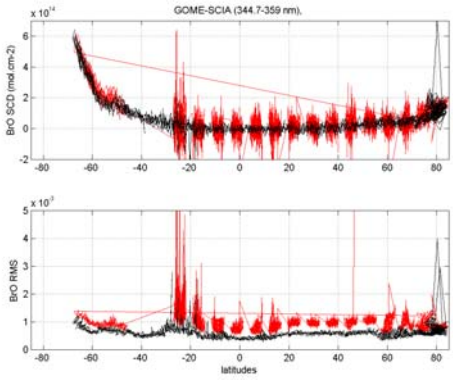

without fit of u2 and u3

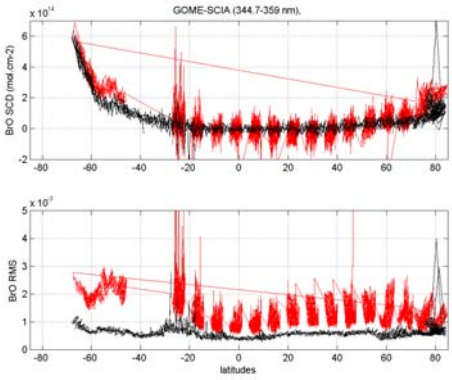

4.4.3 Key data version 2 (Config 3, Processor 4.02b, Nadir key data 3.0)

344.7-359 nm

with fit of u2 and u3

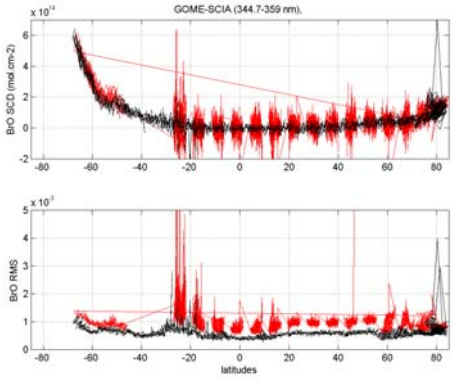

without fit of u2 and u3

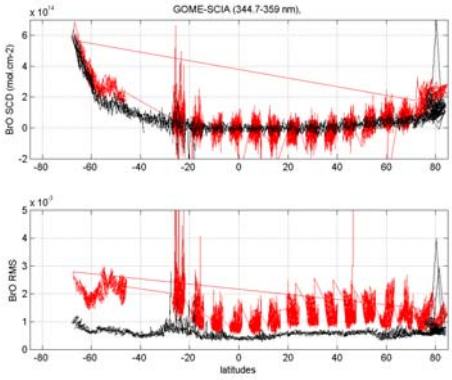

4.4.4 Key data version 3 (Config 4, Processor 4.02b, Nadir key data 2.4)

344.7-359 nm

with fit of u2 and u3

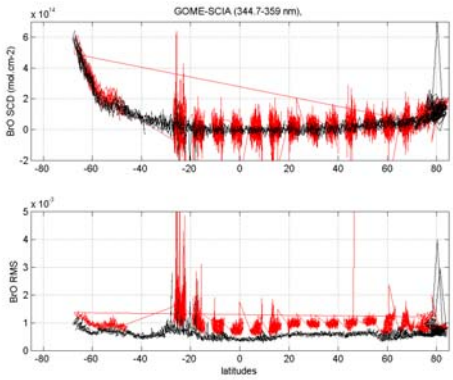

without fit of u2 and u3

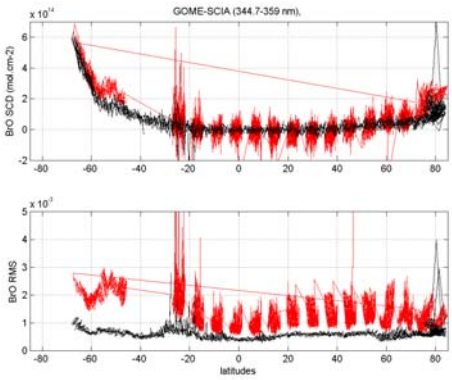

4.5 Orbit 2509, Config 4, Processor 4.02b, Nadir key data 2.4 in the UV-shifted window.

336-351.5 nm

with fit of u2 and u3

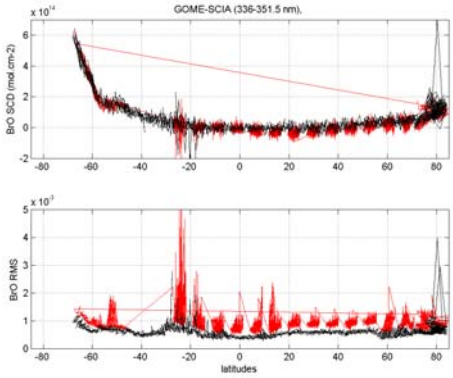

without fit of u2 and u3

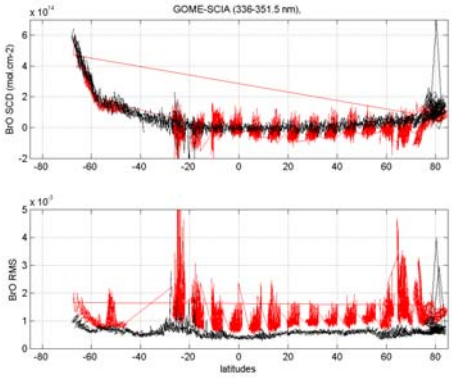

4.6 Fit tests on two pixels of the orbit 2509:

Pixel 3757 can be considered as a "normal" pixel, while pixel 3600 is in the region where RMS are significantly higher when u2 and u3 are not fitted.

4.6.1 Record 3757/4119, SZA: 80.82°, Lat = -61.45, Long = -7.835

4.6.1.1 Config. 1: 344.7-359 nm

Without u2 and u3 fit:

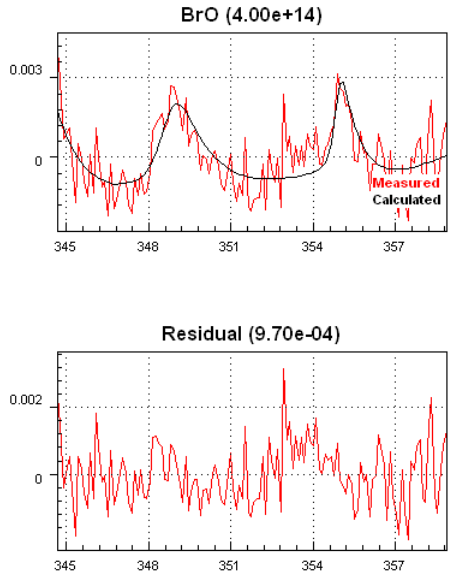

With u2 and u3 fit:

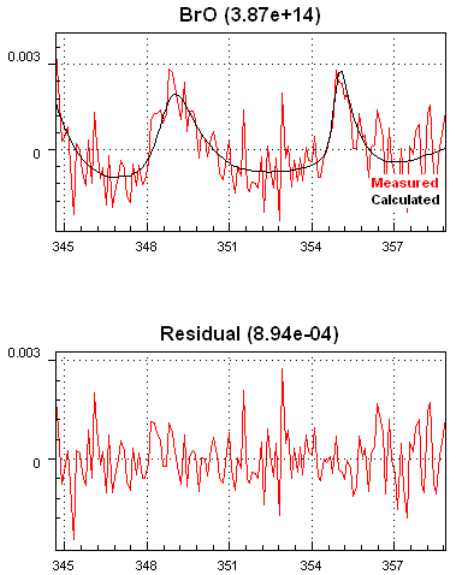

4.6.1.2 Config. 1: 336-351.5 nm

Without u2 and u3 fit:

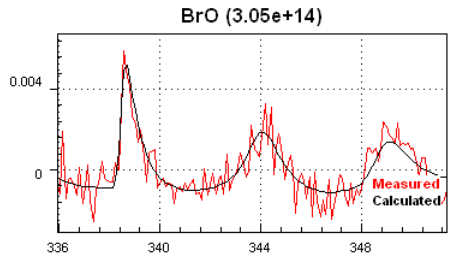

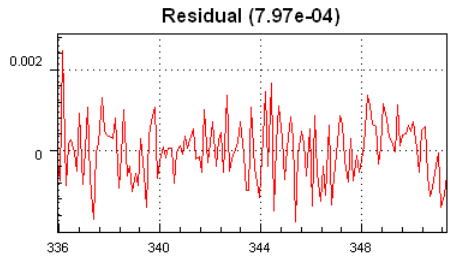

With u2 and u3 fit:

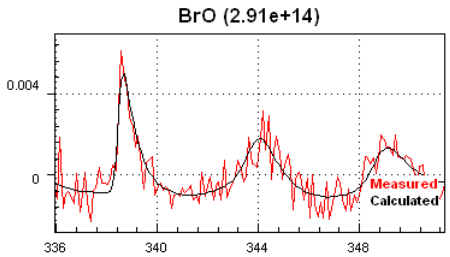

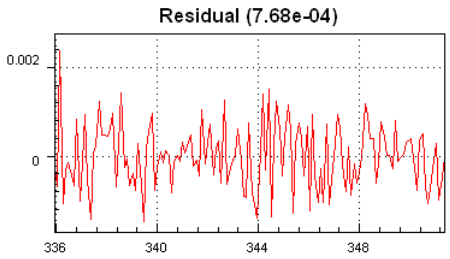

4.6.1.3 Config. 2: 344.7-359 nm

Without u2 and u3 fit:

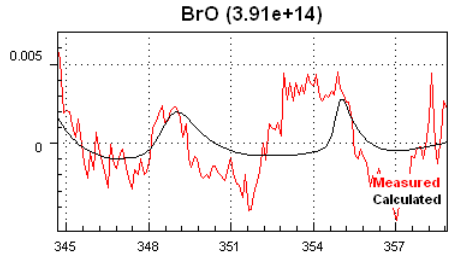

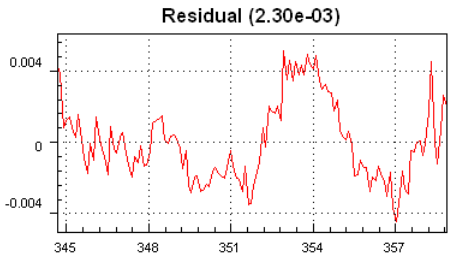

With u2 and u3 fit:

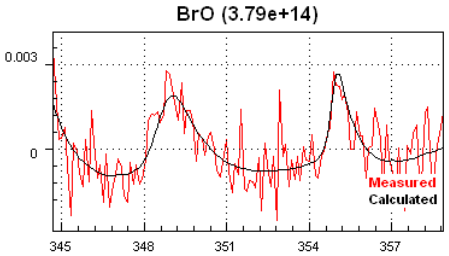

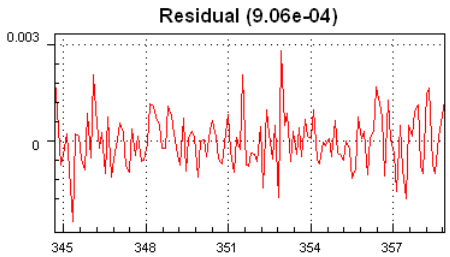

4.6.1.4 Config. 4: 344.7-359 nm

Without u2 and u3 fit:

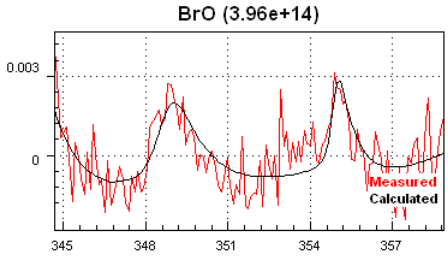

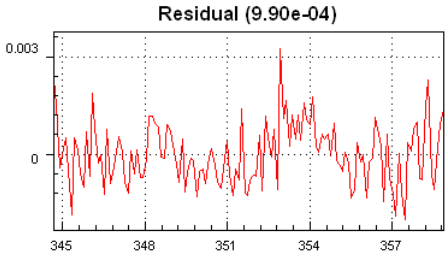

With u2 and u3 fit:

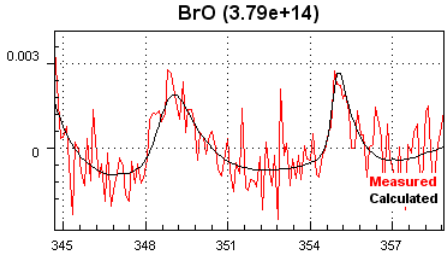

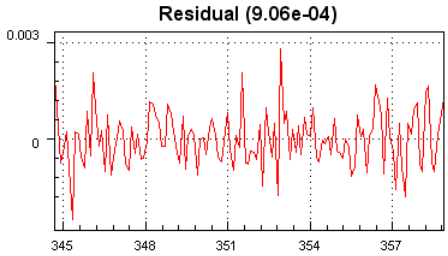

4.6.1.5 Config. 2: 336-351.5 nm

Without u2 and u3 fit:

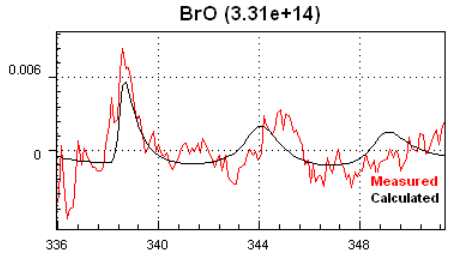

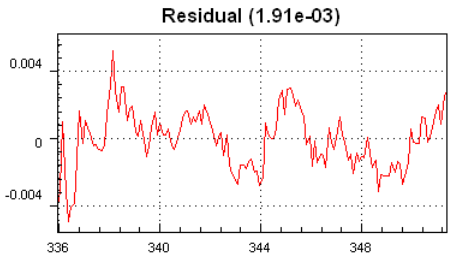

With u2 and u3 fit:

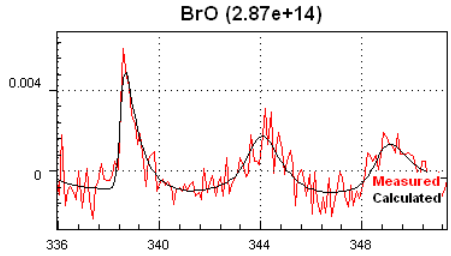

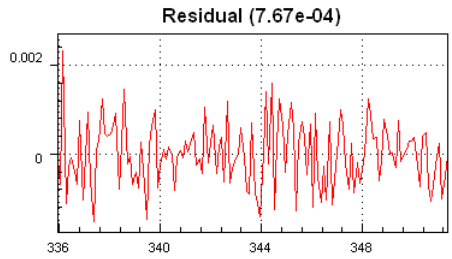

4.6.1.6 Config. 4: 336-351.5nm

Without u2 and u3 fit:

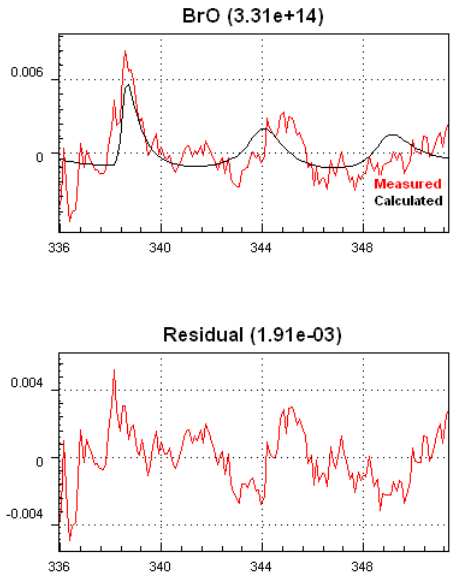

With u2 and u3 fit:

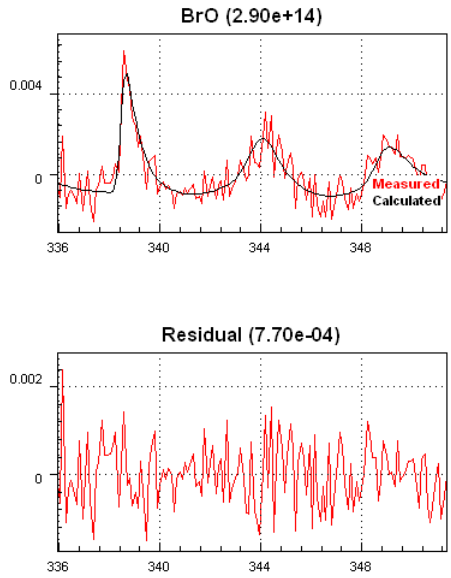

4.6.2 Record 3600/4119, SZA: 72.65°, Lat = -51.68, Long = -4.33

4.6.2.1 Config. 1: 344.7-359 nm

Without u2 and u3 fit:

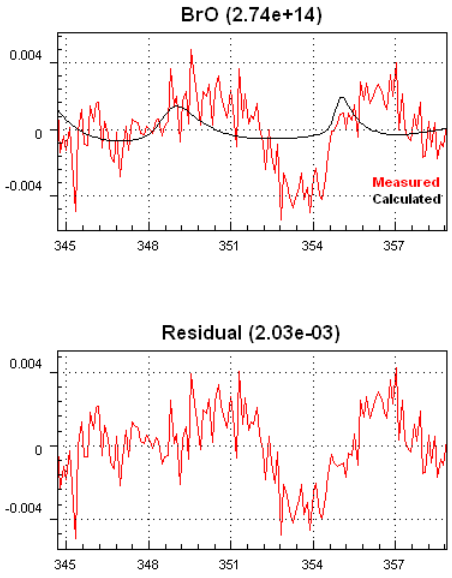

With u2 and u3 fit:

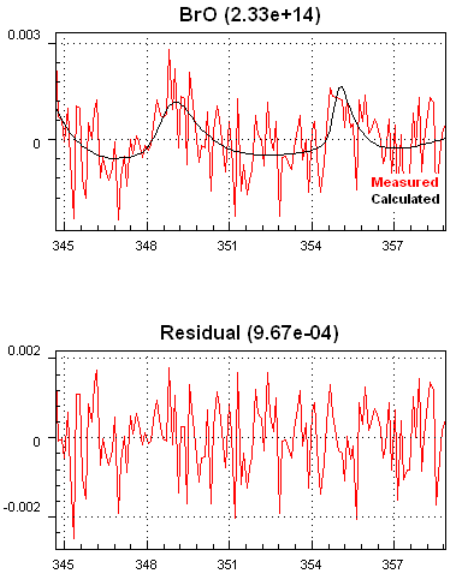

4.6.2.2 Config. 1: 336-351.5 nm

Without u2 and u3 fit:

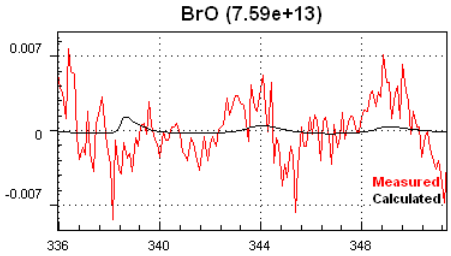

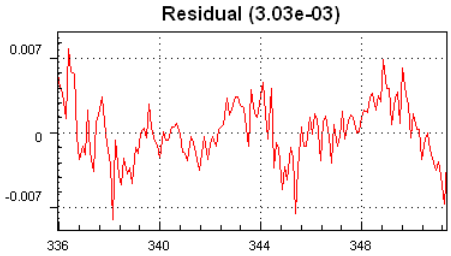

With u2 and u3 fit:

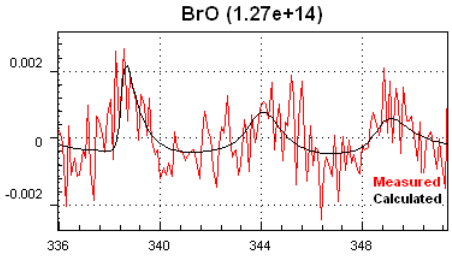

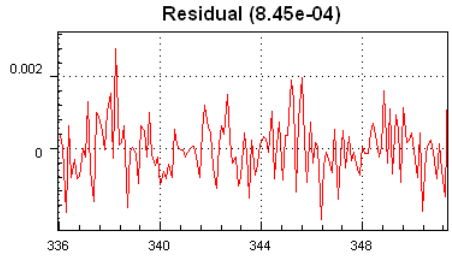

4.6.2.3 Config. 3: 344.7-359 nm

Without u2 and u3 fit:

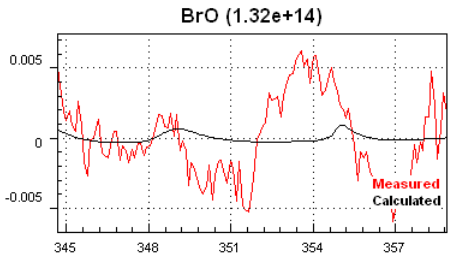

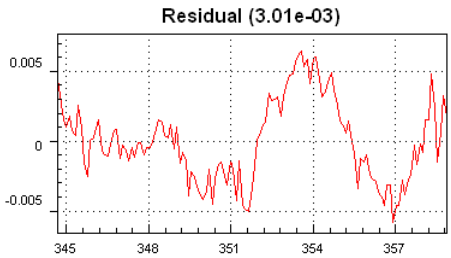

With u2 and u3 fit:

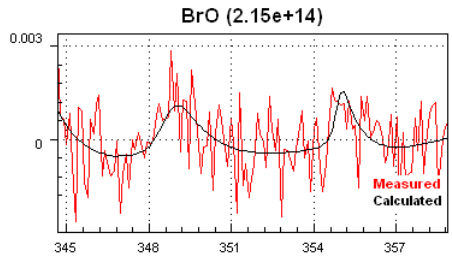

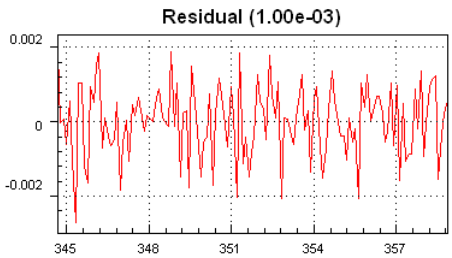

4.6.2.4 Config. 4: 344.7-359 nm

Without u2 and u3 fit:

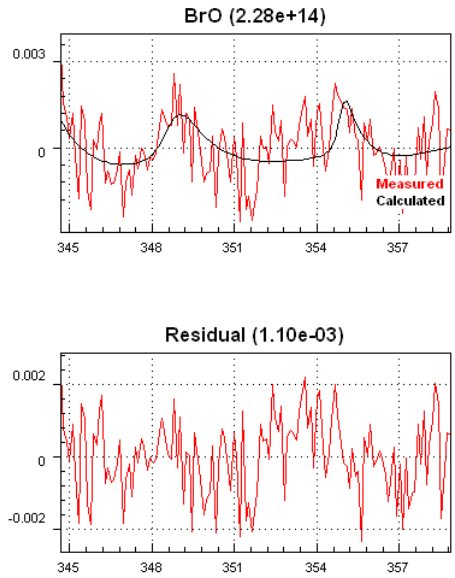

With u2 and u3 fit:

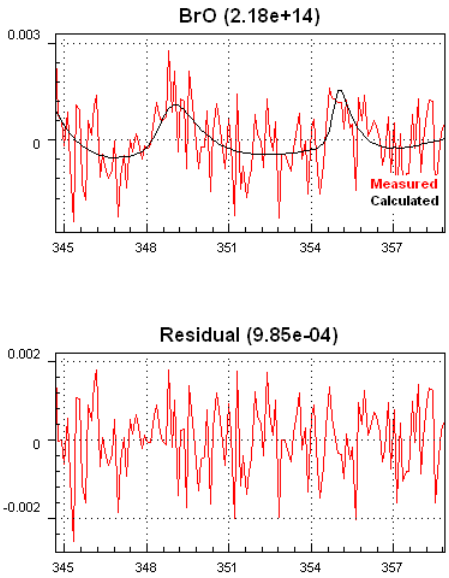

4.6.2.5 Config. 3: 336-351.5 nm

Without u2 and u3 fit:

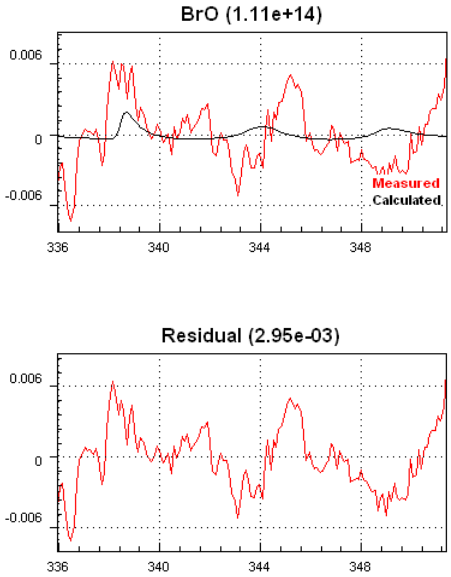

With u2 and u3 fit:

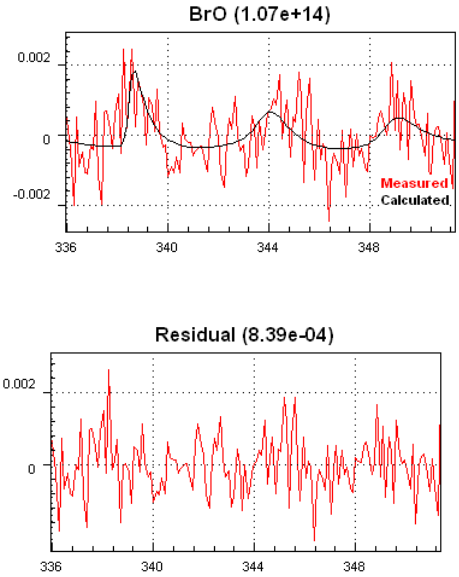

4.6.2.6 Config. 4: 336-351.5nm

Without u2 and u3 fit:

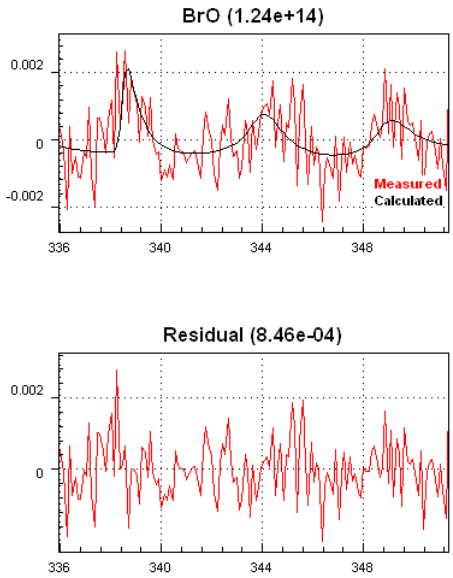

With u2 and u3 fit:

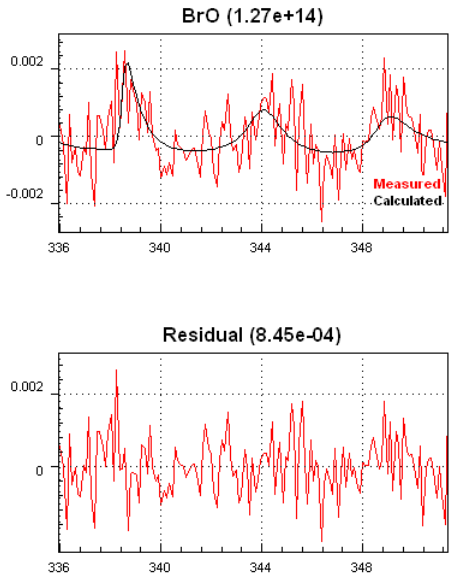

4.7 Conclusions

In all cases, polarization sensitivity vectors *u2 and u3 need to be fitted*. When those are fitted, there is no difference between a calibration with polarization correction (option 6) and without it. Similarly, there is little difference between the different versions of the key data. However, in general, versions 1 and 3 of the key data lead to better results than version 2.

If u2 and u3 are not fitted, previous results (Config. 1) were better when the polarization correction was not applied during calibration. In the opposite, Config. 2 and 4 show better results when the polarization correction is applied during calibration. This suggests that the polarization correction has been improved in the new version of the processor, but not enough to suppress the need of fitting u2 and u3.

As the version 3 of the key data (2.4), with polarization correction, seems to be the best option of the new processor (4.02b), a last test has been made by doing the analysis in 336-351.5 nm to compare this new version with our best configuration until now (config.1 in 366-351.5 nm, with (or without) correction of polarization, with fit of u2 and u3). In this window as well, and for the new version of the processor, polarization sensitivity vectors u2 and u3 need to be fitted.

4.8 References

Aliwell, S.R., M. Van Roozendael, P. V. Johnston, A. Richter, T. Wagner, et al., Analysis for BrO in zenith-sky spectra - An intercomparison exercise for analysis improvement, *J. Geophys. Res., 107*, D14, doi: 10.1029/2001JD000329, 2002.

Boersma, K.F. and Eskes, H.J., GOME Assimilated NO2 Field For Scientific Users And Model Validation, *Geophysical Research Abstracts*, Vol. 5, 05267, 2003.

Burrows, J. P., A. Richter, A. Dehn, B. Deters, S. Himmelmann, S. Voigt, and J. Orphal, Atmospheric remote -sensing-reference data from GOME: 2. Temperature-dependent absorption cross sections of O3 in the 231-794 nm range, *JQSRT, 61,* 509-517, 1999.

Burrows, J. P. , A. Dehn, B. Deters, S. Himmelmann, A. Richter, S. Voigt and J. Orphal, Atmospheric Remote-Sensing Reference Data from GOME: 1. Temperature-Dependent Absorption Cross Sections of NO_2 in the 231-794 nm Range, *JQSRT, 60,* 1025, 1998.

Cantrell, Davidson, McDaniel, Shetter and Calvert, Temperature-Dependent Formaldehyde Cross Sections in the Near-Ultraviolet Spectral Region, *J. Phys. Chem., 94,* 3902-3908, 1990

Chance, K, Analysis of BrO Measurements from the Global Ozone Monitoring Experiment, *Geophys. Res. Lett. 25,* 3335-3338, 1998.

Chipperfield, M.P. et al., Sequential assimilation of stratopheric chemical observations in a three-dimensional model, *J. Geophys. Res., 107,* 4585, 2002.

Chipperfield, M., and J.A. Pyle, Model sensitivity studies of Arctic Ozone Depletion, *J. Geophys. Res., 103,* 28,389-28,403, 1998.

Koelemeijer, R.B.A., A Fast method for retrieval of clouds parameters using oxygen A band measurements from the Global Ozone Monitoring Experiment, *J. Geophys. Res., 106,* 3475-3490, 2001.

Kromminga, H., J. Orphal, S. Voigt and J. P. Burrows, "Fourier-transform-spectroscopy of symmetric chlorine dioxide (OClO)", Proc. EC Advanced Study Course (ASTAIRE 1999), Bergen, Norway, 1999.

Martin, R.V., An improved retrieval of tropospheric nitrogen dioxide from GOME, *J. Geophys. Res, 107,* 4437-4457, 2002.

McElroy, M.B., R.J. Salawitch, S.C. Wofsy, and J.A. Logan, Reductions of Antarctic ozone due to synergistic interactions of chlorine and bromine, *Nature, 321,* 759-762, 1986.

Platt, U., "Differential Optical Absorption Spectroscopy (DOAS)", in *Air Monitoring by Spectroscopic Techniques*, chap. 127, edited by M.W.Sigrist, pp.27-84, John Wiley, New York, 1994.

Richter, A. and Burrows, J.P., Tropospheric NO_2 from GOME measurements, *Adv. Space Res., 29,* 1673-1683, 2002.

Richter, A., F. Wittrock, M. Eisinger, and J.P. Burrows, GOME observations of tropospheric BrO in northern hemispheric spring and summer 1997, *Geophys. Res. Lett., 25,* 2683-2686, 1998.

Richter, A., Wittrock, F., Ladstätter-Weißenmayer, A., and J. P. Burrows, GOME measurements of stratospheric and tropospheric BrO, *Adv. Space Res. 29,* 1673-1683, 2002.

Stamnes, K. et al., Numerically stable algorithm for discrete-ordinate-method radiative transfer in multiple Scattering end emitting layered media, *Applied Optics, 27,* 2502, 1998.

Tanskanen, A. et al., Use of the moving time-window technique to determine surface albedo from the TOMS reflectivity data. Submitted to Proceedings of SPIE, 4896, 2003.

Van Roozendael, M., C. Fayt, J.-C. Lambert, I. Pundt, T. Wagner, A. Richter, and K. Chance, Development of a bromine oxide product from GOME, in Proc. ESAMS'99-European Symposium on Atmospheric Measurements from Space, ESTEC, The Netherlands, 1999, ESA WPP-161, 1999.

Vountas, M., V.V. Rozanov and J.P. Burrows, Ring effect: Impact of Rotational Raman Scattering on Radiative Transfer in Earth's Atmosphere, *JQSRT, 60,* 943, 1998.

Wagner, T., and U. Platt, Satellite mapping of enhanced BrO concentrations in the troposphere, *Nature, 395,* 486-490, 1998.

Wahner, A., et al., *Chem. Phys. Lett., 152,* 507, 1988.

Wilmouth, D. M., T. F. Hanisco, N. M. Donahue, and J. G. Anderson, Fourier Transform Ultraviolet Spectroscopy of the $A(^2\Pi_{3/2}) \leftarrow X(^2\Pi_{3/2})$ Transition of BrO, *J. Phys. Chem., 103,* 8935-8944, 1999.

Annexe : Orbit 2510

4.9 Orbit 2510 with polarization correction during calibration (options: 1,2,3,4,5,6,7)

4.9.1 Previous results (Config. 1, Processor 4.0, Nadir key data 2.2)

344.7-359 nm

with fit of u2 and u3

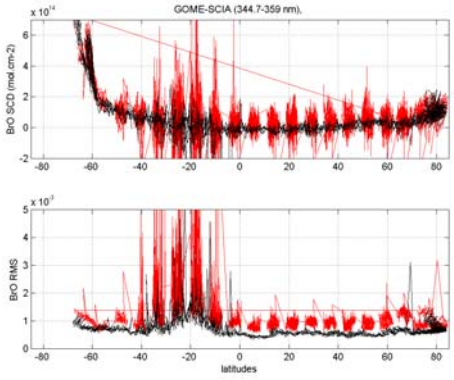

without fit of u2 and u3

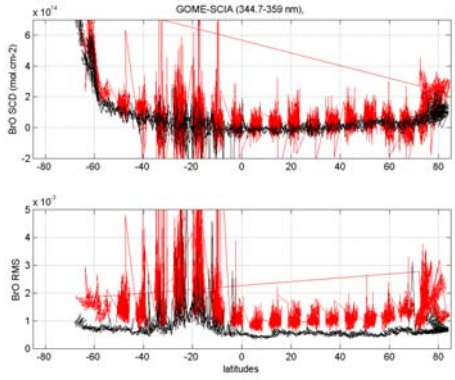

336-351.5 nm

with fit of u2 and u3

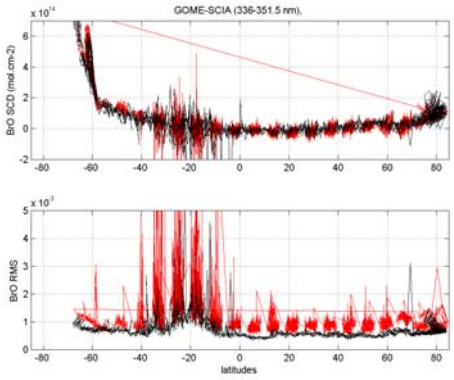

without fit of u2 and u3

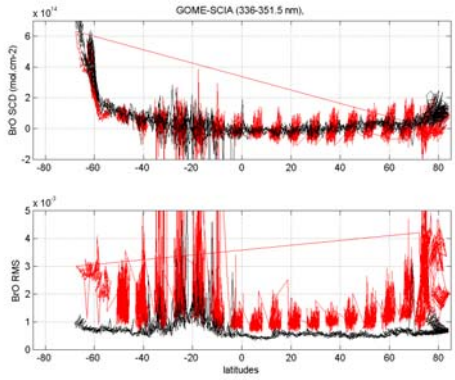

4.9.2 Key data version 1 (Config. 2, Processor 4.02b, Nadir key data 2.2)

344.7-359 nm

with fit of u2 and u3

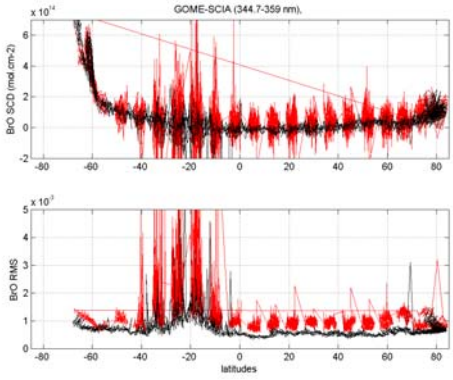

without fit of u2 and u3

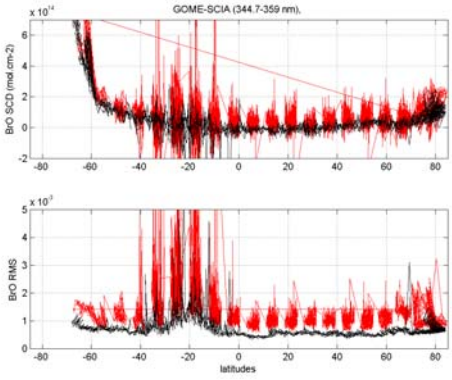

4.9.3 Key data version 2 (Config. 3, Processor 4.02b, Nadir key data 3.0)

344.7-359 nm

with fit of u2 and u3

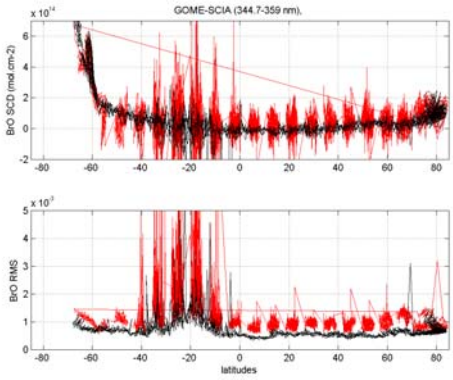

without fit of u2 and u3

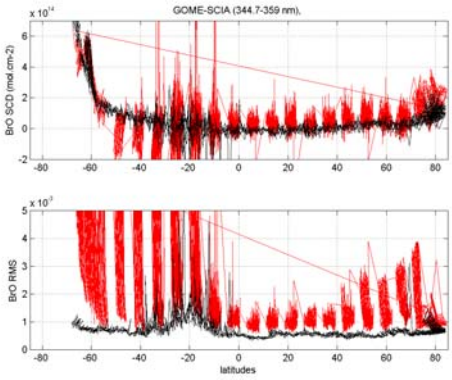

4.9.4 Key data version 3 (Config. 4, Processor 4.02b, Nadir key data 2.4)

344.7-359 nm

with fit of u2 and u3

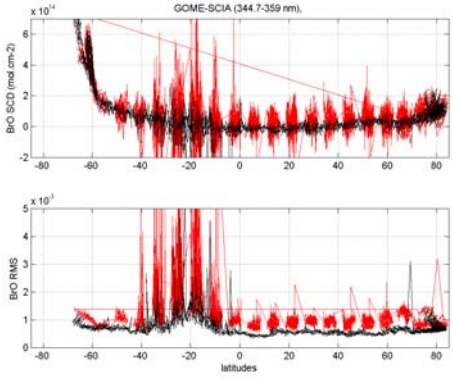

without fit of u2 and u3

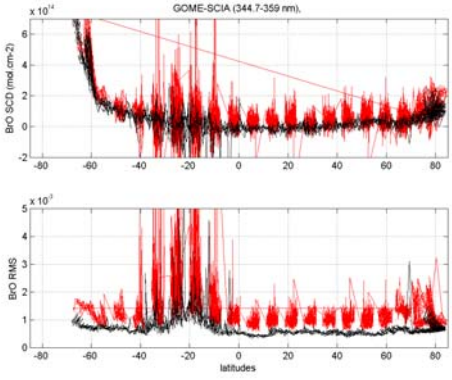

4.10 Orbit 2510 without polarization correction during calibration (options: 1,2,3,4,5,7)

4.10.1 Previous results (Config 1, Processor 4.0, Nadir key data 2.2)

344.7-359 nm

with fit of u2 and u3

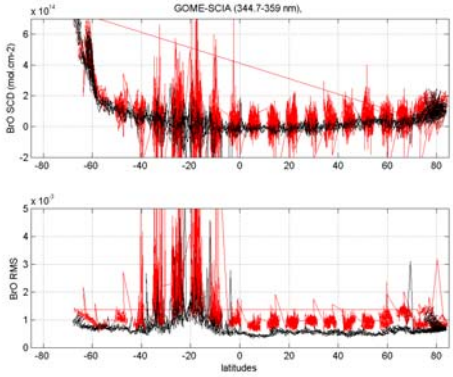

without fit of u2 and u3

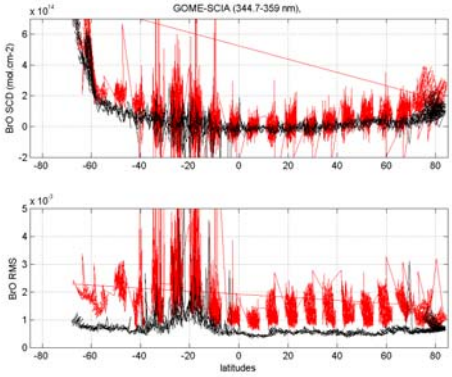

336-351.5 nm

with fit of u2 and u3

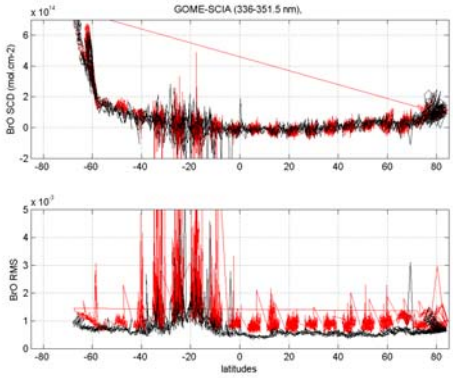

without fit of u2 and u3

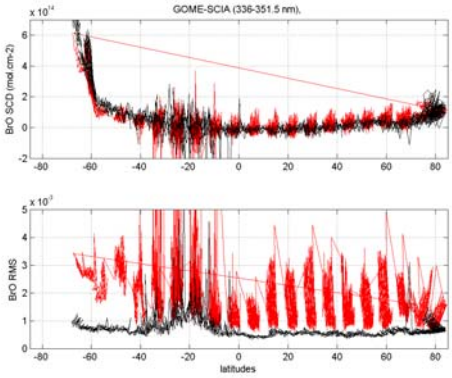

4.10.2 Key data version 1 (Config 2, Processor 4.02b, Nadir key data 2.2)

344.7-359 nm

with fit of u2 and u3

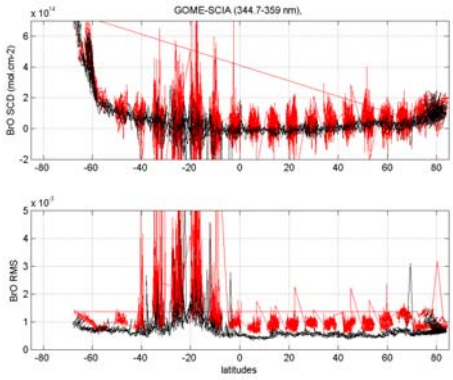

without fit of u2 and u3

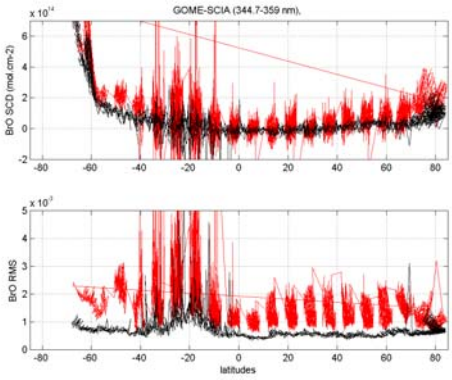

4.10.3 Key data version 2 (Config 3, Processor 4.02b, Nadir key data 3.0)

344.7-359 nm

with fit of u2 and u3

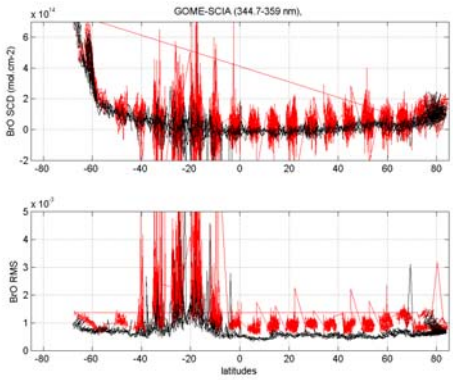

without fit of u2 and u3

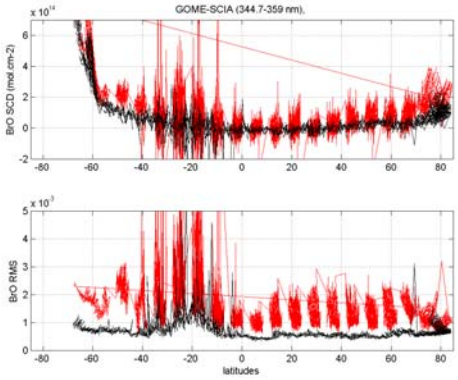

4.10.4 Key data version 3 (Config 4, Processor 4.02b, Nadir key data 2.4)

344.7-359 nm

with fit of u2 and u3

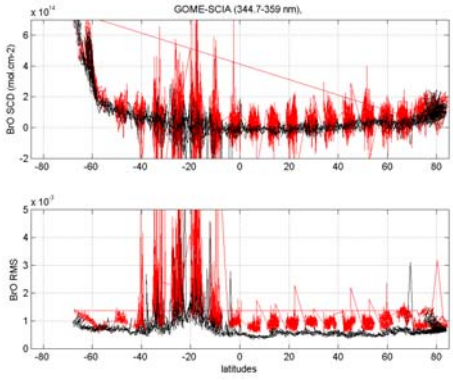

without fit of u2 and u3

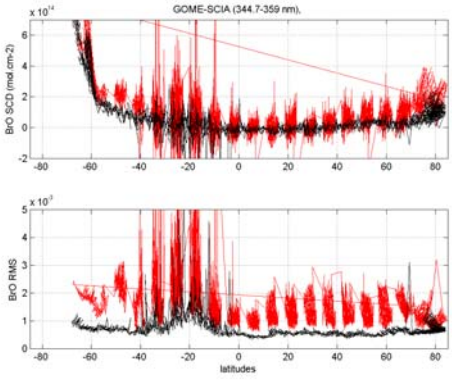

4.11 Config 4, Processor 4.02b, Nadir key data 2.4 in the UV-shifted window.

336-351.5 nm

with fit of u2 and u3

Orbit 2510

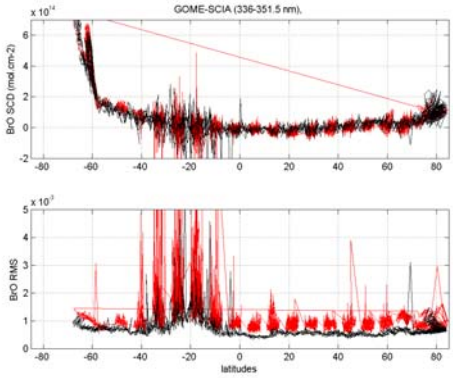

without fit of u2 and u3